AGU PUBLICATIONS

JGR

Journal of Geophysical Research: Space Physics

RESEARCH ARTICLE
10.1002/2015JA021574

Key Points:
- Dynasonde data are used to determine the magnitude and phase of tidal harmonics
- Variability of the first three tidal harmonics between 140 and 300 km altitude
- Existence of several distinct altitude ranges showing higher tidal amplitudes

Correspondence to:
C. Negrea,
Catalin.Negrea@noaa.gov

Citation:
Negrea, C., N. Zabotin, T. Bullett, M. Codrescu, and T. Fuller-Rowell (2016), Ionospheric response to tidal waves measured by dynasonde techniques, *J. Geophys. Res. Space Physics*, *121*, 602–611, doi:10.1002/2015JA021574.

Received 18 JUN 2015
Accepted 21 NOV 2015
Accepted article online 24 NOV 2015
Published online 16 JAN 2016

Ionospheric response to tidal waves measured by dynasonde techniques

Cătălin Negrea[1,2,3,4], Nikolay Zabotin[1,2], Terence Bullett[1,5], Mihail Codrescu[3], and Tim Fuller-Rowell[1,3]

[1]Cooperative Institute for Research in Environmental Sciences, University of Colorado Boulder, Boulder, Colorado, USA, [2]Department of Electrical and Computer Engineering, University of Colorado Boulder, Boulder, Colorado, USA, [3]Space Weather Prediction Center, National Oceanic and Atmospheric Administration, Boulder, Colorado, USA, [4]Institute of Space Science, Magurele, Romania, [5]National Centers for Environmental Information, National Oceanic and Atmospheric Administration, Boulder, Colorado, USA

Abstract Atmospheric tides are known to have a dramatic influence on thermospheric and ionospheric structure and variability. Considerable effort goes into understanding characteristics of tidal modes, their interactions with planetary and gravity waves and other tidal modes, as well as their influence on the background state of the thermosphere-ionosphere system. For the altitude interval between roughly 120 and 400 km, this effort is somewhat hindered by the lack of global observations. We propose a new method of determining tidal variability by making use of dynasonde measurements. The NeXtYZ inversion procedure produces altitude profiles of the ionospheric parameters with a vertical resolution typically better than 1 km. This, together with the typical 2 min cadence of the instrument, results in extensive data sets with wide temporal and altitude coverage. At any given altitude we have nonuniform sampling due to the natural ionospheric variability. A Lomb-Scargle implementation is used to obtain equivalent results at all altitudes and locations. We report height profiles of the first three tidal harmonics derived from dynasonde measurements. The data analyzed include the vertical electron density profiles, the ionospheric *X* (east-west) "tilt" measurement, and the derived zonal plasma density gradient. Both the tilt and the gradient are shown to be sensitive tracers of atmospheric waves. We use data from Wallops Island and San Juan, for two time intervals: 6 May- 6 June and 9 October- 8 November 2013, thus capturing seasonal, latitudinal, and altitude variations of tidal amplitude and phase. This proves the potential of using dynasonde-capable instruments as a data source for tidal studies in the thermosphere.

1. Introduction

Forcings of the thermosphere-ionosphere can be grouped in two categories: solar and geomagnetic forcings and energy and momentum transport by fluid waves from the lower atmosphere [*Forbes*, 1991; *Forbes et al*., 2000; *Akmaev*, 2011]. The second category of forcings can induce periodic fluctuations in the ionospheric plasma density, commonly referred to as traveling ionospheric disturbances (TID). A specific class of which are manifestations of atmospheric thermal waves (tides) with frequencies that are harmonics of 24 h. The relative impact of tides is generally greater during periods of reduced solar activity, but it is always present. The main source of tidal oscillations is known to be the absorption of solar radiation by tropospheric H_2O and stratospheric O_3 [*Groves*, 1982a, 1982b]. These waves propagate upward and increase in amplitude as the background density decreases. Their spectra are modified by nonlinear interactions [*Angelats I Coll and Forbes*, 2002; *Huang et al*., 2012; *Teitelbaum and Vial*, 1991] and by in situ excitation of nonmigrating tidal modes in the thermosphere [*Jones et al*., 2013].

The tides influence background characteristics of the thermosphere-ionosphere system by dumping their momentum into the mean flow as they dissipate and by affecting the wind dynamo in the *E* region. The overall importance of migrating and nonmigrating tidal modes has been amply demonstrated by modeling studies [*Fang et al*., 2013; *Oberheide et al*., 2002, 2009, 2011; *Chen et al*., 2013; *Forbes et al*., 2001; *Hagan and Forbes*, 2002; *Yamazaki and Richmond*, 2013; *Lu et al*., 2012; *Jones et al*., 2013, 2014; *Akmaev et al*., 2008] and, to a lesser extent, by satellite and ground-based data. However, research has been hindered by the so-called "thermospheric gap" in the data [*Oberheide et al*., 2011], referring to the altitude range between 120 and 400 km, for which global tidal measurements are currently sparse. As a result, recent studies using various types of measurements have focused on either the lower thermosphere (below 120 km) or the upper thermosphere (above 400 km) or have used data sets covering short time intervals or limited altitude ranges.

The height profile of tidal harmonics has been studied using incoherent scatter radar measurements [*Huang et al*., 2012; *Gong and Zhou*, 2011; *Hocke*, 1996]. The long-term impact due to tides on the large-scale structure of the ionosphere has been investigated using N_mF_2 data from digisonde stations [*Forbes et al*., 2000], and the global impact of tidal modes has been investigated using satellite observations [*McLandress et al*., 1996]. However, current satellite missions do not provide data above 120 km [*Forbes et al*., 2006; *Warner and Oberheide*, 2014]. A notable exception are the results obtained with Constellation Observing System for Meteorology, Ionosphere, and Climate (COSMIC) data [*Mukhtarov and Pancheva*, 2011], which suggested the presence of several altitude ranges of enhanced ionospheric response to atmospheric tides, below 250 km and above 300 km. Finally, *Häusler et al*. [2015] showed limitations to the existing methodologies for tidal studies reliant on satellite measurements, suggesting a need for ground-based observations. The development we describe here may be considered a response to this need.

We propose the use of dynasonde methods for the study of thermospheric tidal waves. Dynasonde is a generic name for a methodology of precision ionospheric radio sounding [*Wright and Pitteway*, 1979]. The classical principle (detection of radar reflections from ionospheric plasma at frequencies that vary within a sounding session from 0.5 to 25 MHz) is implemented in this technique in a way that puts focus on phase properties of the radio echoes. High-resolution raw data provided by modern digital HF radar hardware with high-performance analog front ends accomplish the precise determination of echo physical parameters. An echo is defined by seven parameters (two angles of arrival, group range, Doppler, polarization, phase range, and amplitude), each with its individual uncertainty estimate determined primarily by ionospheric roughness. Dynasonde analysis yields excellent statistics of recognized echoes (up to several thousands per sounding session). Processing the list of the echo parameters instead of traditional amplitude-based image analysis is another distinctive property of the dynasonde technique. Accuracy of physical parameters (particularly of the range and of the angles of arrival) and rich statistics of recognized echoes provide conditions for a 3-D plasma density inversion procedure, "NeXtYZ," which produces the true vertical profile of plasma density and the vertical profile of horizontal gradients (tilts) [*Zabotin et al*., 2006]. Both characteristics are sensitive to wave activities in the thermosphere-ionosphere system, including manifestations of atmospheric tides. This is because they characterize the local 3-D plasma density, as opposed to the classical vertical height profile, allowing detection of the irregular ionospheric reflection surfaces caused by thermospheric waves.

The purpose of this paper is twofold: first to demonstrate the possibility of using dynasonde methods to fill the current gap in tidal measurements and second to discuss some prominent features of the altitude profiles of amplitude and phase for the major tidal harmonics. The dynasonde compatible instruments can operate continuously. The availability of data sets covering long time periods and broad altitude ranges facilitates the investigation of tidal variability. For this first study, we determine the average height profiles of tidal amplitude and phase for the diurnal, semidiurnal, and terdiurnal tidal harmonics over Wallops Island, VA, and San Juan, PR. This is done for two time intervals: 6 May (11:18) to 6 June (10:50) and 9 October (00:00) to 8 November (23:58), both in 2013. These were chosen such that we would have observations at both locations for 31 uninterrupted days. We capture seasonal, latitude, and altitude variations of the first three tidal harmonics. The *X* (west-east) tilt is our preferred parameter since it is normalized by the magnitude of the electron density gradient (and therefore less dependent on diurnal variations of ionization) and due to the fact that Earth's west-to-east rotation determines the principal direction of propagation of the tidal waves. However, the electron density and *X* (west-east) component of the electron density gradient are also used. Significant tidal amplitudes are present in the *Y* (south-north) tilt data over smaller altitude ranges, but their analysis has not been included in this first publication. Section 2 describes the data used, provides the explanation for the tilts' sensitivity to wave activity, and describes the data analysis methodology. Section 3 discusses amplitude and phase characteristics of tidal harmonics obtained with the new approach employing tilt and associated electron density gradient measurements. Finally, section 4 briefly states our conclusions and future plans.

2. Dynasonde Data Acquisition and Analysis

Wallops Island and San Juan HF radar installations differ somewhat in specific types of transmitting antenna and in layouts of the receiving antenna array, but both are compliants with basic principles of the dynasonde method. Their transmitting antennas provide a broad, vertically directed illumination pattern within the

1–25 MHz frequency band. The receiving arrays consist of eight dipole antennas grouped in two orthogonal lines with antenna separations varying between 10 and 100 m. Careful attention is given to phase calibration of receiving channels. A state-of-the-art digital radar system Vertical Incidence Pulsed Ionospheric Radar (VIPIR) [*Grubb et al*., 2008] performs down conversion and 10 μs sampling of the signal complex amplitude in each channel for a short time window (4480 μs) after every transmitted pulse. Parameters of the sounding session (pulse repetition interval, 5000 μs, and the number of base frequencies, ~580) are set to provide optimal statistics of the echoes on the one hand and an appropriate duration of the session (<2 min) on the other hand. The typical 2 min cadence of the sounding sessions provides sufficient temporal resolution to study wave processes in the ionosphere.

Further processing steps are performed autonomously by the dynasonde analysis software [*Zabotin et al*., 2005]. These include phase-based echo recognition [*Wright and Pitteway*, 1999] and parameterization [*Wright and Pitteway*, 1979], echo classification into traces, and trace selection for higher level analyses. The latter takes advantage of the accurately determined group propagation time and angles of arrival for each ionogram echo. The "stationary phase group range" method provides accuracy down to a few tens of meters [*Paul et al*., 1974]. In addition, a least squares phase comparison method [*Wright and Pitteway*, 1979] permits echo direction-of-arrival calculations with accuracy within 1°. A component of the dynasonde analysis software, the 3-D inversion procedure NeXtYZ, employs multiple ray tracings to reconcile the spatial electron density distribution with the measured echo ranges and their angular positions [*Zabotin et al*., 2006]. The inversion problem is formulated in terms of the recovery of parameters of a parameterized wedge stratified ionosphere (WSI) model that describes locally both the vertical and horizontal gradients of ionospheric plasma density. In the WSI model, the plasma density surfaces are represented locally for small increments in plasma frequency f_p at a sequence of heights h_i along the vertical axis by tilted sections of "frame" planes. The slope of each frame plane is characterized by the two horizontal components n_x, n_y of its normal unit vector (which constitute a mathematical definition of the "tilt"). The two tilts are provided by NeXtYZ as separate outputs as they constitute distinct parameters of the WSI model, separate from the electron density. The normal to the plasma density surface determines the local direction of the total gradient in the layer

$$\vec{n} = (n_x, n_y, n_z) = \frac{\vec{\nabla} N_e}{\left|\vec{\nabla} N_e\right|} . \tag{1}$$

Heights h_i and the components of the normal vector n_x, n_y are found by iterative ray tracing to match the observed ranges and angles of arrival of echoes reflected within the current wedge. The altitude interval for this inversion scheme is determined by the radio echoes detected at the preceding analysis steps; it may extend from the bottom of the *E* layer up to the *F* layer peak.

NeXtYZ produces altitude profiles for several ionospheric parameters: the electron density with associated uncertainties, the *X* (west-east) and *Y* (south-north) tilts and the vertical projection of the line-of-sight Doppler speed characterizing the motion of plasma contours. The original distribution of the profile points is nonuniform, with a typical spacing between adjacent points less than 1 km. For further analysis, all profiles are linearly interpolated to a uniform altitude grid with a 2 km resolution. Time series of the inversion results can be represented in a graphical format, a temporal scan of the vertical ionospheric cross section for a specific parameter. An example of this representation is shown in Figure 1. The two panels use a gray scale to show the *X* tilt as a function of universal time and the altitude for 4 days in October 2013 for the two locations, Wallops Island, VA, and San Juan, PR. One can see a typical diurnal variation in the altitude coverage caused by the solar UV-driven changes in ionospheric ionization. Another prominent feature of the images is the slightly inclined light and dark strips corresponding to periodicities from a few minutes to a few hundred minutes. These are manifestations of traveling ionospheric disturbances most likely caused by ever present gravity waves, with phase fronts propagating downward. A less obvious feature of the images is the presence of long-periodic tilt variations related to tidal harmonics. This feature can be revealed through spectral analysis.

The ionospheric perturbation induced by a superposition of tidal modes is expected to have the following form:

$$N_{em}(z,t) = \sum_s N_{em,s}(z)\ \cos[m\Omega(t - t_m(z)) + sl], \tag{2}$$

where m is a subharmonic of 1 day, s is the zonal wave number, $N_{em,s}$ is the amplitude of a single mode, l is the longitude (expressed in rad), $\Omega = \frac{2\pi}{24\ \mathrm{h}}$ is the Earth's rotation frequency, t is the local time in hours, and t_m is the

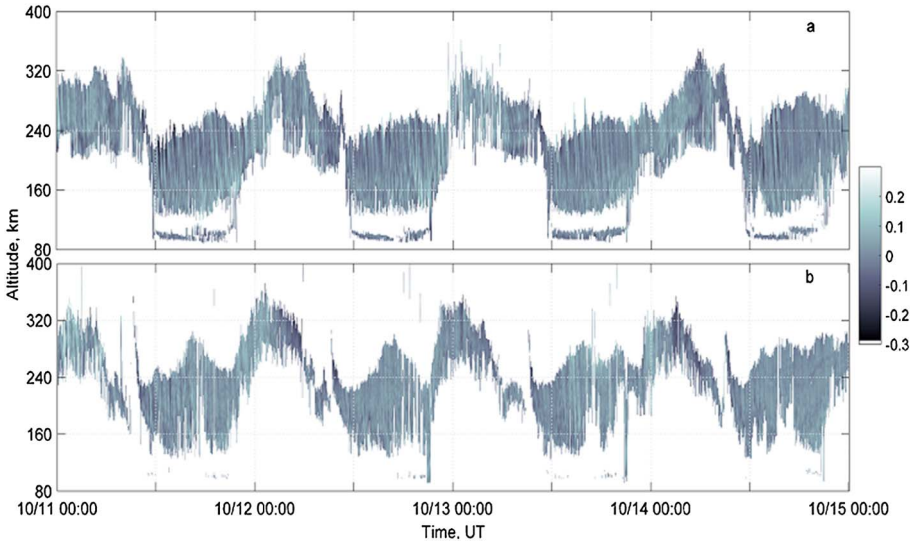

Figure 1. Temporal and altitude variability of the tilts. The two panels use a gray scale to show the west-east tilt n_x as a function of the universal time and the altitude for 4 days in October 2013 for two locations, (a) Wallops Island, VA, and (b) San Juan, PR.

local time corresponding to the maximum of subharmonic m. It is obvious that if a neutral atmosphere oscillation induces an ionospheric response with the time dependence described by equation (2), the electron density gradient, and implicitly also the associated tilt, must exhibit similar oscillatory behavior

$$\nabla_x N_e(z,t) = -\frac{1}{R_E^* \cos(\Phi)} \sum_s s\, N_{em,s}(z)\ \sin[m\Omega(t - t_m(z)) + sl], \tag{3}$$

where R_E is the radius of the Earth and Φ is the latitude. It is possible that a local variation in electron density may be mistakenly attributed to a tidal mode. This is less likely to be the case for the tilt measurement since this is indicative of the spatial structure over a large surface within the stations' field of view. There is a simple relationship between the horizontal and vertical components of the gradient and the tilt values

$$\nabla_x N_e(z,t) = \frac{n_x \nabla_z N_e}{\sqrt{1 - n_x^2 - n_y^2}}. \tag{4}$$

Note that all quantities present in the right-hand side of equation (4) (the tilts and the vertical component of gradient) are available as products of the NeXtYZ inversion.

We used data from the Wallops Island (37.85°N, 75.47°W) and San Juan (18.45°N, 66.07°W) dynasondes. The X tilt and the electron density profiles are direct products of dynasonde analysis, while the X component of the gradient was derived using equation (4). All three quantities are expected to be susceptible to the tidal phenomena, as may be concluded from equations (1)–(3). The time periods used are 31 days from 6 May to 6 June 2013 and 31 days from 9 October to 8 November 2013. Analyses for the two locations were entirely independent. Each spectral harmonic in the spectra is the result of superposition of several tidal modes, propagating both eastward and westward, and in the case of the diurnal variation, superimposed with the tidal effects is the normal diurnal ionospheric variation due to changes in ionization from daytime to nighttime.

Common spectral analysis tools (for example, Fast Fourier Transform) are unsuitable for use with the data. There are several reasons for this. First, the distribution of the data points is nonuniform because of inevitable presence of data gaps. These are mostly caused by ionospheric variability and, to a much lesser extent, by failures of the autonomous analysis procedure. Second, the data are characterized by different samplings at different altitudes. Third, there are differences in the day-to-day ionospheric variability at the two locations. Segments of the data series shown in Figure 1 give a good idea of the mentioned data properties. The spectral analysis tool that we need has to provide objectively comparable results for different time periods, different altitudes, and different locations. The Lomb-Scargle periodogram technique [*Scargle*, 1982, 1989]

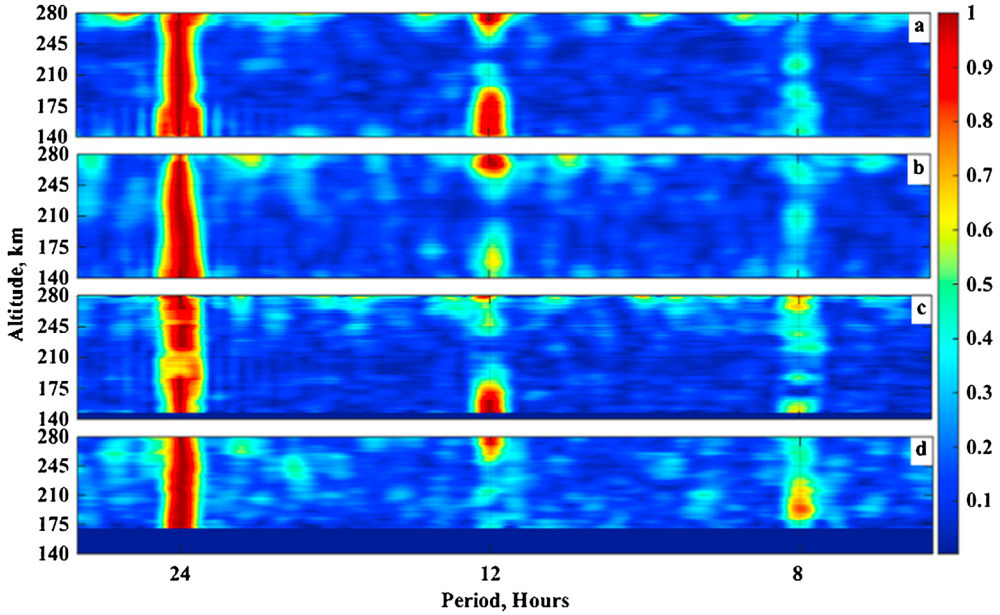

Figure 2. Normalized periodograms of the west-east ionospheric tilt obtained by the dynasonde-based technique for Wallops Island, VA, (a) October and November and (b) May and June 2013 and San Juan, PR, (c) October and November and (d) May and June 2013. One can clearly see the diurnal, semidiurnal, and terdiurnal harmonics in a very broad altitude range.

satisfies all the requirements. The Lomb-Scargle implementation we use is based on that developed by *Hocke and Kämpfer* [2009]; it allows simultaneous determination of both magnitude and phase of Fourier equivalent spectra. The technique was modified slightly to work for an arbitrary set of frequencies. When determining the amplitude, the algorithm was applied to data segments obtained with a sliding Welch [*Welch*, 1967] window of 20 days and a 12 h step; the results were averaged over all 23 steps. The phase was determined in a single step, using the entire 31 day time interval, due to the fact that the Welch method has traditionally only been used to calculate spectral amplitudes and due to the known high variability of the phase of tidal modes [*Murphy*, 2002].

The gap configuration specific to dynasonde data introduces an added difficulty. For most constant altitudes, the size of the data gap can be as large as 12 h for a 24 h interval. This still allows for an accurate fit for the semidiurnal and terdiurnal harmonics. However, *Zhou et al*. [1997] and *Gong et al*. [2013] showed possible errors in the case of the diurnal harmonic, even with the use of the Lomb-Scargle method. While a comprehensive solution to this problem is beyond the scope of this paper, a partial solution is used. *Zhou et al*. [1997] suggest that a tidal harmonic is questionable if it has a small amplitude and random phase variation. In order to avoid such dubious results, at each altitude, a tidal harmonic is considered relevant if its amplitude is 3 times the standard deviation above the mean amplitude. Figure 2 uses color scale to show the Lomb-Scargle results for the *X* tilts as a function of the period and altitude. For this illustration, each periodogram (for every altitude) was independently calculated and normalized by its maximum value. One can clearly see the ability of the dynasonde-based technique to reveal major tidal harmonics in a very broad altitude range.

3. Properties of the Tidal Harmonics

Equation (2) was initially introduced to describe tidal oscillations directly caused by absorption of solar radiation [*Chapman and Lindzen*, 1970]. Some other processes are known to cause oscillations with the same periods, sometimes being referred to as "pseudotides," as opposed to the solar thermal tides [*Vadas et al*., 2014; *Walterscheid et al*., 1986]. In this paper, we broadly refer to all Fourier coefficients corresponding to harmonics of 24 h as "tidal" amplitudes. The diurnal tidal harmonic ($m = 1$) is superimposed over the variability of photoionization, usually resulting in the overestimation of the diurnal tidal harmonic when a nondiscriminative approach is used. Note however that, while the distortion of the diurnal harmonic describing electron density variations is

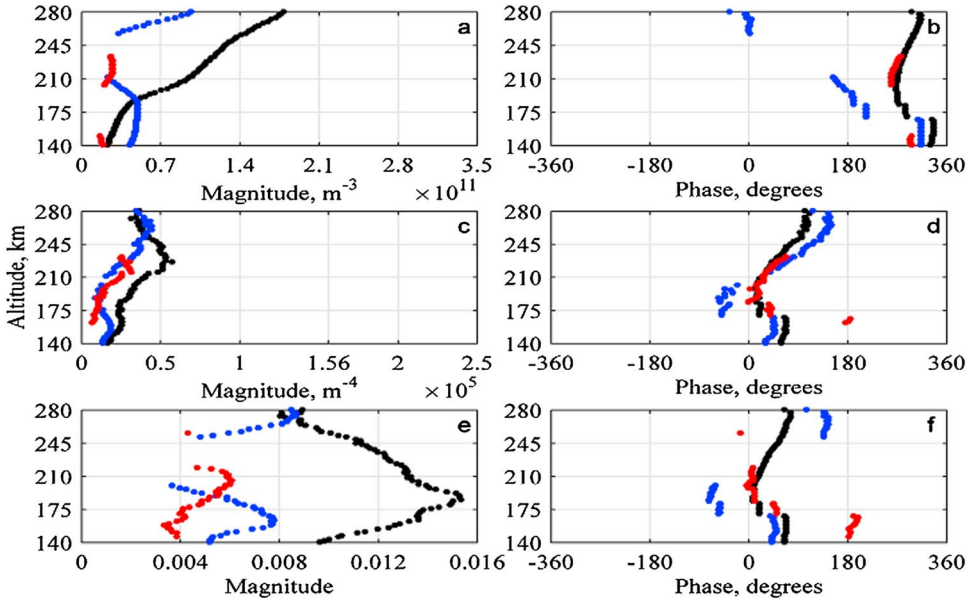

Figure 3. (a, c, and e) Amplitude and (b, d, and f) phase height profiles for the diurnal (black), semidiurnal (blue), and terdiurnal (red) harmonics in the electron density variations (Figures 3a and 3b), in the west-east gradient (Figures 3c and 3d), and in the west-east tilt (Figures 3e and 3f) at Wallops Island, VA, for May and June 2013.

expected to be significant, the effect of photoionization on the tilts and gradients is much smaller. A numerical investigation of this difference can be accomplished, but it is beyond the scope of the present publication.

The set of Figures 3–6 illustrates altitude dependencies of the amplitude and phase of the three major tidal harmonics as revealed by our analysis for the two locations and the two periods. We provide numerical results for all three physical quantities that were previously introduced as possible indicators of the tidal oscillations: electron density, tilts and horizontal gradients.

The structure of the height profiles corresponding to each of the three harmonics may be explained by simultaneous manifestation of several tidal modes with the same frequency. Each mode is likely to have one or

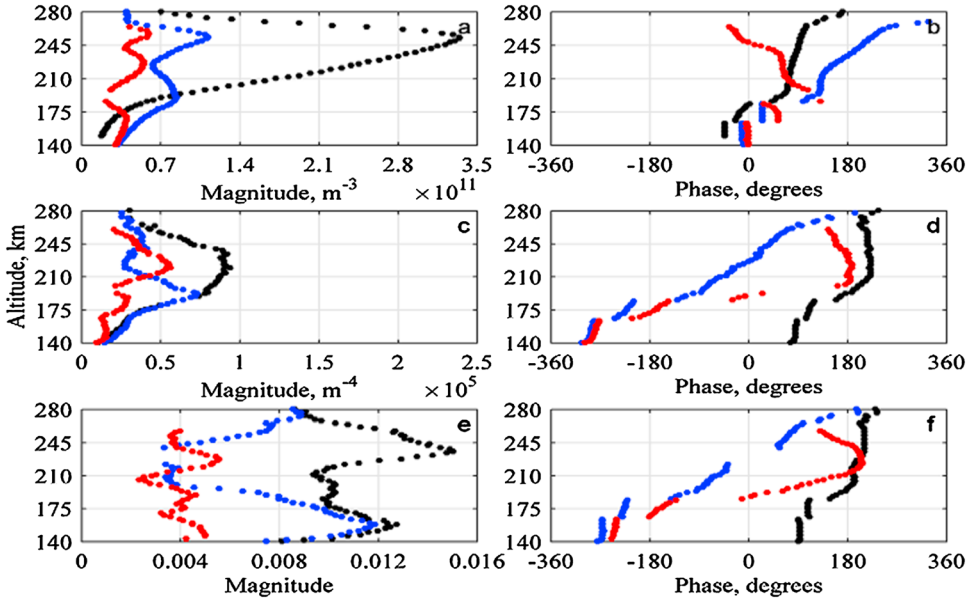

Figure 4. Same as in Figure 3 but for October and November 2013.

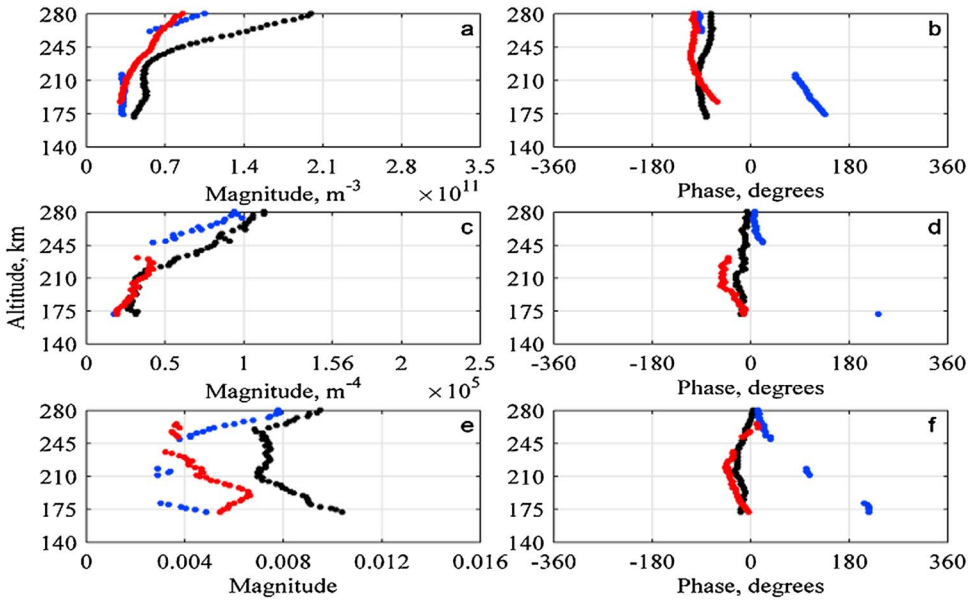

Figure 5. Same as in Figure 3 but at San Juan, PR, and for May and June 2013.

more maxima and minima, their height distributions may vary depending on the zonal wavenumber. One possibility is that a single mode may have a dominant contribution to the amplitude of its corresponding harmonic. In such cases, the summation on the right-hand side in equations (2) and (3) reduces to a single term, and the phase shift between the electron density and its gradient is expected to be either $\frac{\pi}{2}$ or $-\frac{\pi}{2}$ for a westward or eastward propagating mode, respectively. Examples of this behavior may be found in Figure 3 for the diurnal and semidiurnal harmonics below 175 km, Figure 4 for the terdiurnal harmonic between 210 and 240 km, and in Figure 5 for the diurnal harmonic above 180 km and the semidiurnal harmonic above 260 km. For a superposition of waves, equations (2) and (3) suggest that this can no longer be the case, particularly if modes propagating in both directions are present. The altitude profiles of the phase show significant jumps, such as in Figure 3f for the terdiurnal harmonic between 175 and 185 km and in Figure 4b for the terdiurnal harmonic at 195 km. A smooth variation of the phase with altitude indicates the presence of wave modes covering the entire altitude range being considered, as can be observed in Figure 5 for the terdiurnal harmonic. By contrast, the phase jumps indicate significant differences between the wave modes present above and below the jump. Possible explanations are interference of several modes with different height profiles and/or a manifestation of different tidal excitation mechanisms [*Jones et al.*, 2013; *Walterscheid et al.*, 1986].

Phase variation with height is indicative of vertical propagation of the respective tidal harmonic. A typical feature of tidal and gravity waves is that the vertical phase speed must have an opposite sign to that of the vertical component of the group velocity. As such, the phase increase and decrease with height is indicative of downward and upward propagation, respectively. The phase results for the electron density, electron density gradient, and west-east tilt are not necessarily in agreement, and this is explained by the differences between equations (2) and (4). The propagation direction for the diurnal harmonic should not be determined exclusively based on the phase results obtained for electron density due to the potential bias introduced by the diurnal variation in photoionization. At Wallops Island, Figures 3b, 3d, and 3f show downward propagation of the diurnal harmonic between 270 km and 210 km and possibly also downward propagation for the semidiurnal harmonic within the same height interval. For the period of October - November, Figures 4b, 4d, and 4f show downward propagation for the diurnal harmonic between 180 and 280 km, while the terdiurnal harmonic is propagating upward above 240 km and downward below 215 km. At San Juan, during the time interval in May - June 2013, our results (Figures 5b, 5d, and 5f) showed only small phase variations for the diurnal and terdiurnal harmonics. Finally, Figures 6b, 6d, and 6f indicate upward propagation for the semidiurnal harmonic between 180 and 210 km and downward propagation for the terdiurnal harmonic above 210 km.

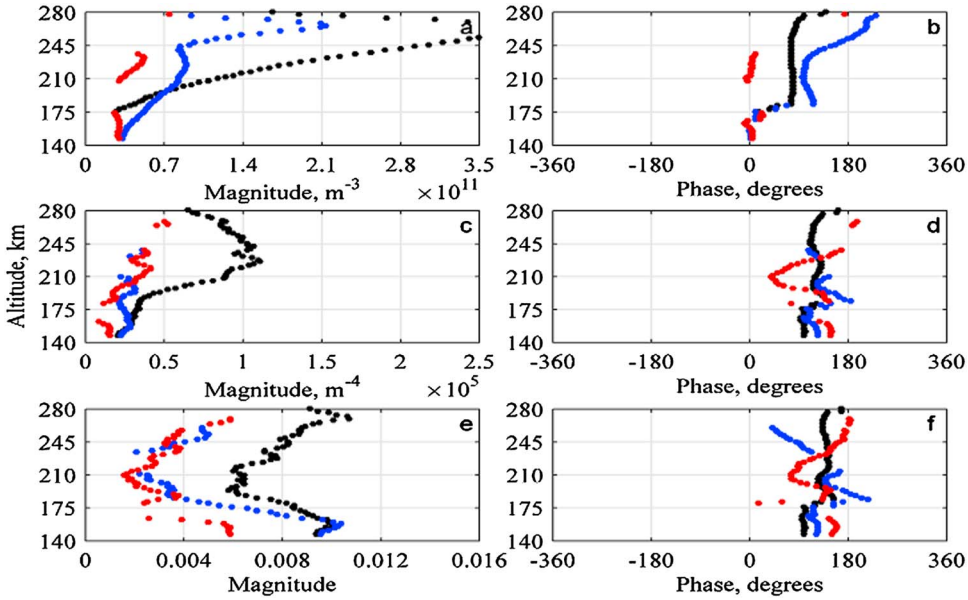

Figure 6. Same as in Figure 5 but for October and November 2013.

Tidal signatures show significant altitude and seasonal variability at both locations. The semidiurnal harmonic at Wallops Island exhibits two altitude ranges of enhanced amplitude: below 200 km and above 245 km. This is valid for both data sets, and such a feature has been previously reported [*Mukhtarov and Pancheva*, 2011]. The particular data sets used here indicate that the separation between the two regions may be as small as 50 km. The terdiurnal harmonic at Wallops Island in October - November exhibits at least three maxima. By combining information in Figures 4a, 4c, and 4e four such distinct maxima can be identified. The amplitude of the semidiurnal and terdiurnal harmonics in the electron density at Wallops Island varies between 0.5×10^{1}–1×10^{11} and 0.2×10^{11}–0.6×10^{11} m^{-3}, respectively. At San Juan, the semidiurnal and terdiurnal harmonics exhibit amplitudes of 0.2×10^{11}–2.1×10^{11} and 2×10^{11}–0.8×10^{11} m^{-3}, respectively. The range for the amplitudes of both the semidiurnal and terdiurnal harmonics is similar to those previously reported by *Mukhtarov and Pancheva* [2011].

4. Conclusions

We report estimates of the amplitude and phase of the first three tidal harmonics at thermospheric altitudes using dynasonde analysis. Our results are based on data obtained at Wallops Island, VA, and San Juan, PR, for May - June and October - November 2013. The plasma density and *X* tilt variations are sensitive indicators of tidal oscillations. We also derive and use for the same purpose the local west-east gradient of the plasma density. Electron density amplitudes of approximately 10^{10}–10^{11} m^{-3} are obtained at both locations but with significant differences observed in the altitude structure of the harmonics. The semidiurnal and terdiurnal harmonics show two or more local maxima in amplitude. Possible causes are simultaneous manifestation of several modes with the same frequency and/or existence of several excitation mechanisms. This may particularly be true when the abrupt phase shifts are observed at altitudes between consecutive maxima.

This study demonstrates a possibility to infer ionospheric features caused by tidal modes using dynasonde data. Global measurements of atmospheric tides are currently not available, and local measurements have been scarce and until now only covering short time intervals. The methodology used in this study can be extended for other dynasonde-capable instruments. An important feature of the HF radars, lacking for other ground-based instruments, is their ability to operate continuously with low operational costs. Long-term studies are thus possible covering a broad geographical latitude interval. This provides a way to "fill" the gap for tidal measurements in the thermosphere.

The tilt measurement is particularly useful in detecting tidal and wave features in general, as it is sensitive to wave-like perturbations and explicitly normalized. Like the plasma density, it is however an ionospheric and not a thermospheric characteristic. One possible way to address this would be a semiempirical approach describing the thermosphere-ionosphere coupling.

Acknowledgments
This work was supported by grant NNX11A061G from the National Aeronautics and Space Administration and by the Office of Naval Research Basic Research Challenge program, award N000141310348. The dynasonde data were obtained freely from the National Centers for Environmental Information (ftp://ftp.ngdc.noaa.gov/ionosonde/data/WI937/ for Wallops Island and ftp://ftp.ngdc.noaa.gov/ionosonde/data/SJJ18/ for San Juan). The authors would like to thank R.A. Akmaev for helpful discussions.

References

Akmaev, R. A. (2011), Whole atmosphere modeling: Connecting terrestrial and space weather, *Rev. Geophys.*, *49*, RG4004, doi:10.1029/2011RG000364.

Akmaev, R. A., T. J. Fuller-Rowell, F. Wu, J. M. Forbes, X. Zhang, A. F. Anghel, M. D. Iredell, S. Moorthi, and H.-M. Juang (2008), Tidal variability in the lower thermosphere: Comparison of Whole Atmosphere Model (WAM) simulations with observations from TIMED, *Geophys. Res. Lett.*, *35*, L03810, doi:10.1029/2007GL032584.

Angelats i Coll, M., and J. M. Forbes (2002), Nonlinear interactions in the upper atmosphere: The $s = 1$ and $s = 3$ nonmigrating semidiurnal tides, *J. Geophys. Res.*, *107*(A8), 1157, doi:10.1029/2001JA900179.

Chapman, S., and R. S. Lindzen (1970), *Atmospheric Tides: Thermal and Gravitational*, 200 pp., Gordon and Breach, New York.

Chen, C. H., C. H. Lin, L. C. Chang, J. D. Huba, J. T. Lin, A. Saito, and J. Y. Liu (2013), Thermospheric tidal effects on the ionospheric midlatitude summer nighttime anomaly using SAMI3 and TIEGCM, *J. Geophys. Res. Space Physics*, *118*, 3836–3845, doi:10.1002/jgra.50340.

Fang, T.-W., R. Akmaev, T. Fuller-Rowell, F. Wu, N. Maruyama, and G. Millward (2013), Longitudinal and day-to-day variability in the ionosphere from lower atmosphere tidal forcing, *Geophys. Res. Lett.*, *40*, 2523–2528, doi:10.1002/grl.50550.

Forbes, J. (1991), Middle atmosphere tides and coupling between atmospheric regions, *J. Geomagn. Geoelectr.*, *43*, 597–609, doi:10.5636/jgg.43.Supplement2_597.

Forbes, J. M., S. E. Palo, and X. Zhang (2000), Variability of the ionosphere, *J. Atmos. Sol. Terr. Phys.*, *62*(8), 685–693.

Forbes, J. M., X. Zhang, and M. E. Hagan (2001), Simulations of diurnal tides due to tropospheric heating from the NCEP/NCAR Reanalysis Project, *Geophys. Res. Lett.*, *28*, 3851–3854, doi:10.1029/2001GL013500.

Forbes, J. M., J. Russell, S. Miyahara, X. Zhang, S. Palo, M. Mlynczak, C. J. Mertens, and M. E. Hagan (2006), Troposphere-thermosphere tidal coupling as measured by the SABER instrument on TIMED during July–September 2002, *J. Geophys. Res.*, *111*, A10S06, doi:10.1029/2005JA011492.

Gong, Y., and Q. Zhou (2011), Incoherent scatter radar study of the terdiurnal tide in the *E*- and *F*-region heights at Arecibo, *Geophys. Res. Lett.*, *38*, L15101, doi:10.1029/2011GL048318.

Gong, Y., Q. Zhou, and S. Zhang (2013), Atmospheric tides in the low-latitude *E* and *F* regions and their responses to a sudden stratospheric warming in January 2010, *J. Geophys. Res. Space Physics*, *118*, 7913–7927, doi:10.1002/2013JA019248.

Groves, G. V. (1982a), Hough components of ozone heating, *J. Atmos. Terr. Phys.*, *44*, 111–121.

Groves, G. V. (1982b), Hough components of water vapour heating, *J. Atmos. Terr. Phys.*, *44*, 281–290.

Grubb R. N., R. Livingston, and T. W. Bullett (2008), A new general purpose high performance HF Radar, Paper GH-4, URSI GA, August 7–16, Chicago, Ill. [Available at http://www.ursi.org/proceedings/procGA08/ papers/GHp4.pdf.]

Hagan, M. E., and J. M. Forbes (2002), Migrating and nonmigrating diurnal tides in the middle and upper atmosphere excited by tropospheric latent heat release, *J. Geophys. Res.*, *107*(D24), 4754, doi:10.1029/2001JD001236.

Häusler, K., M. E. Hagan, J. M. Forbes, X. Zhang, E. Doornbos, S. Bruinsma, and G. Lu (2015), Intraannual variability of tides in the thermosphere from model simulations and in situ satellite observations, *J. Geophys. Res. Space Physics*, *120*, 751–765, doi:10.1002/2014JA020579.

Hocke, K. (1996), Tidal variations in the high-latitude E and F region observed by EISCAT, *Ann. Geophys.*, *14*, 201–210, doi:10.1007/s00585-996-0201-9.

Hocke, K., and N. Kämpfer (2009), Gap filling and noise reduction of unevenly sampled data by means of the Lomb-Scargle periodogram, *Atmos. Chem. Phys.*, *9*, 4197–4206, doi:10.5194/acp-9-4197-2009.

Huang, C., S. Zhang, Q. Zhou, F. Yi, and K. Huang (2012), Atmospheric waves and their interactions in the thermospheric neutral wind as observed by the Arecibo incoherent scatter radar, *J. Geophys. Res.*, *117*, D19105, doi:10.1029/2012JD018241.

Jones, M., Jr., J. M. Forbes, M. E. Hagan, and A. Maute (2013), Non-migrating tides in the ionosphere-thermosphere: In situ versus tropospheric sources, *J. Geophys. Res. Space Physics*, *118*, 2438–2451, doi:10.1002/jgra.50257.

Jones, M., Jr., J. M. Forbes, M. E. Hagan, and A. Maute (2014), Impacts of vertically propagating tides on the mean state of the ionosphere-thermosphere system, *J. Geophys. Res. Space Physics*, *119*, 2197–2213, doi:10.1002/2013JA019744.

Lu, X., H.-L. Liu, A. Z. Liu, J. Yue, J. M. McInerney, and Z. Li (2012), Momentum budget of the migrating diurnal tide in the Whole Atmosphere Community Climate Model at vernal equinox, *J. Geophys. Res.*, *117*, D07112, doi:10.1029/2011JD017089.

McLandress, C., G. G. Shepherd, and B. H. Solheim (1996), Satellite observations of thermospheric tides: Results from the wind imaging interferometer on UARS, *J. Geophys. Res.*, *101*, 4093–4114, doi:10.1029/95JD03359.

Mukhtarov, P., and D. Pancheva (2011), Global ionospheric response to nonmigrating DE3 and DE2 tides forced from below, *J. Geophys. Res.*, *116*, A05323, doi:10.1029/2010JA016099.

Murphy, D. J. (2002), Variations in the phase of the semidiurnal tide over Davis, Antarctica, *J. Atmos. Sol. Terr. Phys.*, 1069–1081.

Oberheide, J., M. E. Hagan, R. G. Roble, and D. Offermann (2002), Sources of nonmigrating tides in the tropical middle atmosphere, *J. Geophys. Res.*, *107*(D21), 4567, doi:10.1029/2002JD002220.

Oberheide, J., J. M. Forbes, K. Häusler, Q. Wu, and S. L. Bruinsma (2009), Tropospheric tides from 80 to 400 km: Propagation, interannual variability, and solar cycle effects, *J. Geophys. Res.*, *114*, D00I05, doi:10.1029/2009JD012388.

Oberheide, J., J. M. Forbes, X. Zhang, and S. L. Bruinsma (2011), Climatology of upward propagating diurnal and semidiurnal tides in the thermosphere, *J. Geophys. Res.*, *116*, A11306, doi:10.1029/2011JA016784.

Paul, A. K., J. W. Wright, and L. S. Fedor (1974), The interpretation of ionospheric radio drift measurements—VI. Angle-of-arrival and group path [echolocation] measurements from digitized ionospheric soundings: The group-path vector, *J. Atmos. Terr. Phys.*, *36*(2), 193–214.

Scargle, J. D. (1982), Studies in astronomical time series analysis. II. Statistical aspects of spectral analysis of unevenly spaced data, *Astrophys. J.*, *263*, 835–853.

Scargle, J. D. (1989), Studies in astronomical time series analysis. III. Fourier transforms, autocorrelation and cross-correlation functions of unevenly spaced data, *Astrophys. J.*, *343*, 874–887.

Teitelbaum, H., and F. Vial (1991), On tidal variability induced by nonlinear interaction with planetary waves, *J. Geophys. Res.*, *96*(A8), 14,169–14,178, doi:10.1029/91JA01019.

Vadas, S. L., H.-L. Liu, and R. S. Lieberman (2014), Numerical modeling of the global changes to the thermosphere and ionosphere from the dissipation of gravity waves from deep convection, *J. Geophys. Res. Space Physics*, *119*, 7762–7793, doi:10.1002/2014JA020280.

Walterscheid, R. L., G. G. Sivjee, G. Schuberatnd, and R. M. Hamwey (1986), Large-amplitude semidiurnal temperature variations in the polar mesopause: Evidence of a pseudotide, *Nature*, *324*, 347–349.

Warner, K., and J. Oberheide (2014), Nonmigrating tidal heating and MLT tidal wind variability due to the El Niño–Southern Oscillation, *J. Geophys. Res. Atmos.*, *119*, 1249–1265, doi:10.1002/2013JD020407.

Welch, P. D. (1967), The use of fast Fourier transform for the estimation of power spectra: A method based on time averaging over short, modified periodograms, *IEEE Trans. Audio Electroacoust.*, *15*(2), 70–73, doi:10.1109/TAU.1967.1161901.

Wright, J. W., and M. L. V. Pitteway (1979), Real-time data acquisition and interpretation capabilities of the Dynasonde: 1. Data acquisition and real-time display, *Radio Sci.*, *14*(5), 815–825, doi:10.1029/RS014i005p00815.

Wright, J. W., and M. L. V. Pitteway (1999), A new data acquisition concept for digital ionosondes: Phase-based echo recognition and real-time parameter estimation, *Radio Sci.*, *34*, 871–882, doi:10.1029/1999RS900039.

Yamazaki, Y., and A. D. Richmond (2013), A theory of ionospheric response to upward-propagating tides: Electrodynamic effects and tidal mixing effects, *J. Geophys. Res. Space Physics*, *118*, 5891–5905, doi:10.1002/jgra.50487.

Zabotin, N. A., J. W. Wright, T. W. Bullett, and L. Y. Zabotina (2005), Dynasonde 21 principles of data processing, transmission, storage and web service Proceedings of the Ionospheric Effects Symposium 2005, edited by J. M. Goodman, pp. 7B3-1–7B3-3, Alexandria, Va.

Zabotin, N. A., J. W. Wright, and G. A. Zhbankov (2006), NeXtYZ: Three-dimensional electron density inversion for dynasonde ionograms, *Radio Sci.*, *41*, RS6S32, doi:10.1029/2005RS003352.

Zhou, Q. H., M. P. Sulzer, and C. A. Tepley (1997), An analysis of tidal and planetary waves in the neutral winds and temperature observed at low-latitude *E* region heights, *J. Geophys. Res.*, *102*, 11,491–11,505, doi:10.1029/97JA00440.